Appendix B

INVERSION OF THE n_e PROFILE BY USING THE ZERNICKE POLYNOMIAL TECHNIQUE

The equilibrium reconstruction code ODIN, using the equilibrium magnetic measurements alone, is able to produce a correct identification of the magnetic topology that labels the plasma by a flux function ψ^{ODIN} (Fig. 32, full lines, shot No. 2728); however, it cannot provide the exact value of the flux function ψ, which is better approximated by the flux function ψ^{ODINP} produced by the conditioned code ODINP (Fig. 32, dashed lines). Nevertheless, the real flux function ψ is, within a reasonable approximation, a function of ψ^{ODIN}; this is even true for a high q_ψ shot like No. 2728 (Fig. 33) where, as discussed in Section 2, the discrepancy between ODIN and ODINP is among the largest so far obtained. Correspondingly, as, in an MHD equilibrium without plasma flows, the pressure is a function of the flux function $P(\psi)$ and moreover as, in the collisionless high temperature regime, the very high parallel thermal conductivity makes the temperature a function of ψ, the electron density must also be a function of ψ, $n_e = n_e(\psi)$. Consequently, one can assume that $n_e = n_e(\psi^{\text{ODIN}})$ for all practical purposes concerning the inversion of the interferometric line integrated signals: in the remainder of this Appendix, as well as in the main body of the paper, no other distinction will be maintained between ψ and ψ^{ODIN} in the matter of the n_e profile.

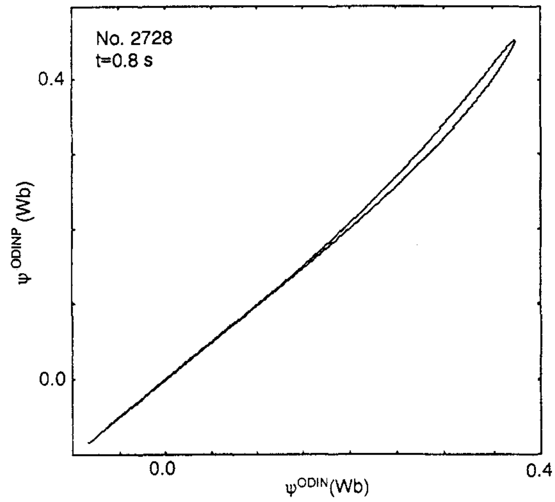

FIG. 33. Shot No. 2728 at t = 0.8 s. Relationship between ψ^{ODINP} and ψ^{ODIN} of Fig. 32, as observed on the midplane Z = 0.

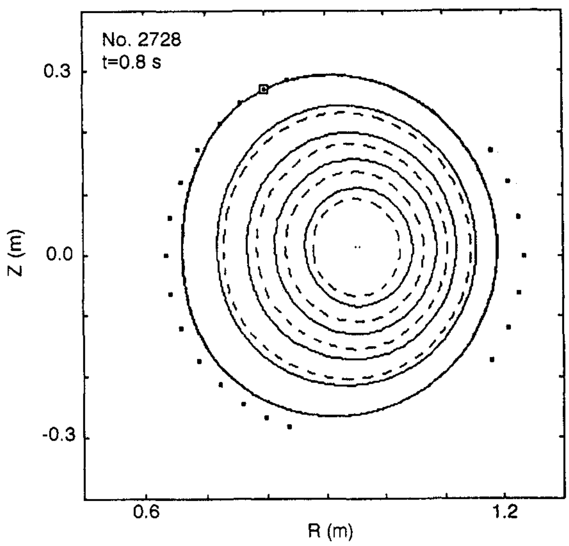

FIG. 32. Shot No. 2728 at t = 0.8 s. Contour map of the poloidal flux function ψ^{ODIN}, as identified from the unconditioned code ODIN: the solid curves correspond to $\psi^{ODIN} = k\psi^{ODIN}_{axis}/5$, with k = 0 to 5. Contour map of the poloidal flux function ψ^{ODINP}, as identified from the kinetic–magnetic code ODINP: the dashed curves correspond to $\psi^{ODINP} = k\psi^{ODIN}_{axis}/5$ and k = 0 to 5. The tips of the 'mushrooms' of the poloidal limiters are shown as points and the limiter–plasma contact point is identified by a small square.

The determination of the functional form of $n_e(\psi)$ from a limited number of interferometric signals is performed by a truncation of the power expansion,

$$n_e(\psi) = n_0 + \sum_{k=1}^{K} n_k \psi^{k/2} \tag{7}$$

The choice of expanding $n_e(\psi)$ in terms of $\psi^{1/2}$, and not in terms of ψ, comes from the result that, in the large majority of cases in which the electron density profile is not peaked, the density profile behaves essentially like $\psi^{1/2}$, and so a description in terms of integer powers of ψ would require too many terms.

The channels of the DCN interferometer [25] measure the line integrated densities

$$D_j = \int_{l_j} n_e \, dl_j$$

along the vertical chords at $R = R_j$ with length l_j through the FTU plasma; as there are just five of these, a very limited number K of coefficients n_k in formula (7) can be determined.

The technique of inversion is based on the Zernicke polynomials [26–28], of angular order m and radial order l, that are defined on the polar co-ordinates (ρ, η) of the unitary circle as

$$Z_m^l(\rho) = \sum_{s=0}^{l} (-1)^s \begin{pmatrix} m+2l-s \\ m+l-s \end{pmatrix} \begin{pmatrix} l \\ s \end{pmatrix} \rho^{m+2l-2s} \quad (8)$$

These polynomials constitute a good basis for comparing local quantities $g(\rho, \eta)$ over the unit circle with their line integrated values $f(p, \phi)$ along a chord with impact parameter p and impact angle ϕ. The correspondence between components of the angular (respectively, η and ϕ) Fourier expansions $g_m^{c/s}(\rho)$ and $f_m^{c/s}(p)$ is

$$g_m^{c/s}(\rho) = \sum_{l=0}^{\infty} (m+2l+1) a_m^{l,c/s} Z_m^l(\rho) \quad (9a)$$

$$f_m^{c/s}(p) = 2 \sum_{l=0}^{\infty} a_m^{l,c/s} \sin[(m+2l+1)\cos^{-1}(p)] \quad (9b)$$

The reconstructed equilibrium is enclosed within a Zernicke circle, centred on the plasma magnetic axis $(R_{\rm axis}, Z_{\rm axis})$, with a radius $R_{\rm d}$ that includes the plasma boundary. The half-integer powers of the flux function $\psi^{k/2}$ are expanded in Zernicke polynomials with respect to this circle,

$$\psi^{k/2}(\rho, \eta) = \sum_{m=0}^{M} \sum_{l=0}^{L} (m+2l+1) \times (a_m^{l,c}(k)\cos(m\eta) + a_m^{l,s}(k)\sin(m\eta)) Z_m^l(\rho) \quad (10)$$

The truncation of the expansion is set to $M = 6$, $L = 11$, which guarantees an accuracy of 1% on ψ. Fictitious measurement chords inside the Zernicke circle, with zero line integrated densities, have to be added outside the plasma as a regularization of the oscillatory behaviour of the high order Zernicke polynomials. Using Eq. (7), where the density at the boundary n_0 is set to 10% of the central chord of the DCN interferometer, and adding eight zero-measurement chords outside the plasma, the following overdetermined system is solved for $j = 1, 13$ (5 DCN chords + 8 zero chords):

$$(D_j - n_0 l_j)/R_d = 2 \sum_{k=1}^{K} n_k \left[\sum_{m=0}^{M} \sum_{l=0}^{L} [a_m^{l,c}(k)\cos(m\phi_j) + a_m^{l,s}(k)\sin(m\phi_j)] \sin[(m+2l+1)\cos^{-1}(p_j)] \right] \quad (11)$$

where p_j and ϕ_j are the impact parameters and the

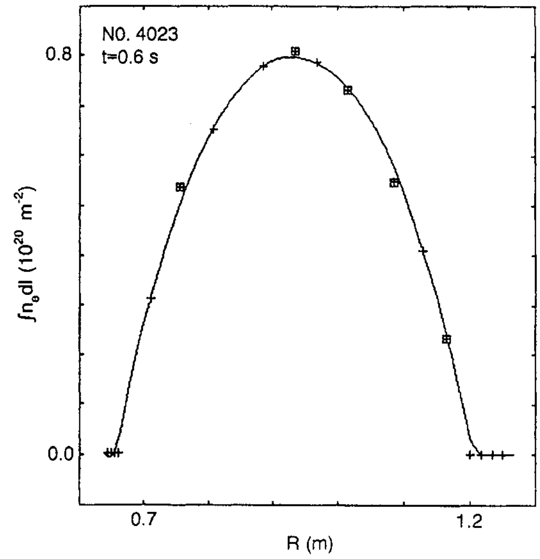

FIG. 34. Shot No. 4023 at t = 0.6 s. Line integrated densities $D_j = \int_{l_j} n_e \, dl_j$, along the vertical chords at $R = R_j$ with length l_j through the FTU plasma, as measured from the DCN interferometer chords (squares), as calculated on the flux function mirrored chords after the preliminary inversion (crosses), along with zero chords outside the plasma (crosses). They are compared with the line integral of the final density inversion $n_e(\psi) = n_0 + n_1\psi^{1/2} + n_2\psi + n_3\psi^{3/2}$, shown as a solid line as a function of the major radius on the symmetry plane $Z = Z_{axis}$ of the plasma.

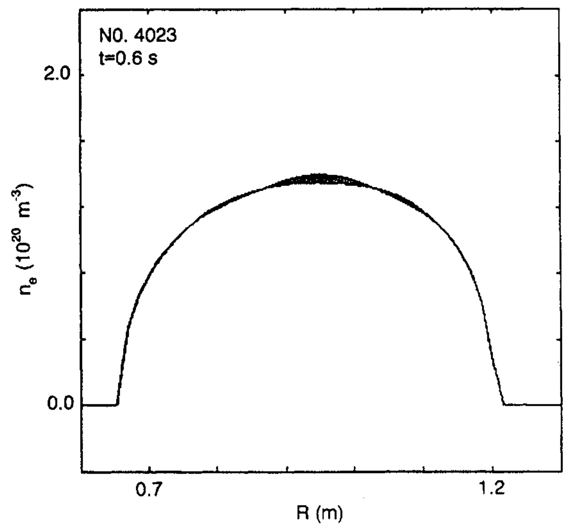

FIG. 35. Inverted electron density profile, on the symmetry plane $Z = Z_{axis}$ of the plasma, for shot No. 4023 at t = 0.6 s. The shaded region shows the uncertainty due to two different choices for the parametrization of $n_e(\psi)$, $n_0 + n_1\psi^{1/2} + n_2\psi + n_3\psi^{3/2}$ and $n_0 + n_1\psi^{1/2} + n_4\psi^{4/2} + n_5\psi^{5/2}$, respectively.

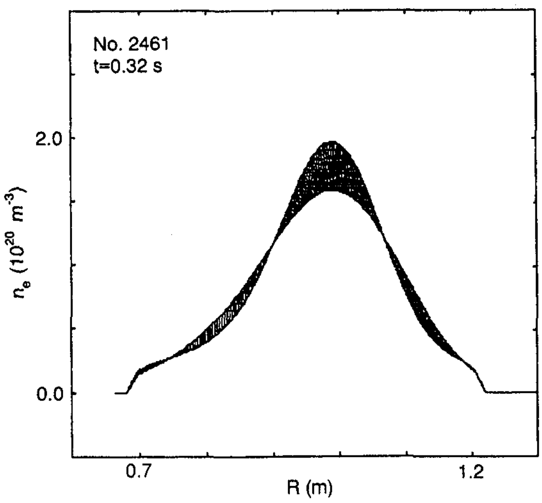

FIG. 36. Inverted electron density profile, on the symmetry plane $Z = Z_{axis}$ *of the plasma, for shot No. 2461 at* $t = 0.32$ *s, characterized by a plasma detachment phenomenon. The shaded regions show the uncertainty due to two different choices for the parametrization of* $n_e(\psi)$, $n_0 + n_1\psi^{1/2} + n_2\psi + n_3\psi^{3/2}$ *and* $n_0 + n_1\psi^{1/2} + n_4\psi^{4/2} + n_5\psi^{5/2}$, *respectively.*

angles of the measurement chords reduced to the unit Zernicke circle: $p_j = |R_j - R_{\text{axis}}|/R_{\text{d}}$, $\phi_j = 0$ if $R_j \geq R_{\text{axis}}$, $\phi_j = \pi$ if $R_j < R_{\text{axis}}$.

The system (11) is solved, by minimizing the sum of the squares of the mismatch of every equation, at first with $K = 2$; then the five measurement points are mirrored with respect to the magnetic axis, based on the result of the first inversion, and system (11) is finally solved for $j = 1, 18$ (5 DCN chords + 8 zero chords + 5 mirrored chords) with $K = 3$; this procedure will be referred to as the standard choice for

$$n_{\text{e}}(\psi) = n_0 + n_1\psi^{1/2} + n_2\psi^{2/2} + n_3\psi^{3/2}$$

which is Eq. (4).

An example of the fit for the line integrated electron density is shown in Fig. 34 for shot No. 4023. The choice of using the lowest exponents in Eq. (7) after $\psi^{1/2}$ is arbitrary: in order to investigate a selection of higher exponents, inversions that use

$$n_{\text{e}}(\psi) = n_0 + n_1\psi^{1/2} + n_4\psi^{4/2} + n_5\psi^{5/2}$$

have been performed (the non-standard choice). The inverted electron density profile is shown in Fig. 35 for shot No. 4023, both for the standard and for the non-standard choice for the exponents of $n_{\text{e}}(\psi)$.

Whereas the low and medium q_ψ discharges have broad density profiles and very small uncertainties, the high q_ψ discharges exhibit more peaked density profiles and so larger uncertainties. The discharges characterized by a plasma detachment phenomenon, such as shot No. 2461, exhibit the most peaked density profiles and the uncertainty in the density inversion, due to the choice of the exponents, becomes rather large (see Fig. 36).

ACKNOWLEDGEMENTS

The authors would like to thank the entire FTU team. Particular acknowledgements are due to A. Cecchini, F. Crisanti, D. Fabiani, M. Gasparotto, A. Grosso, E. Lunadei, S. Mantovani, A. Marra, G.B. Righetti and S. Viselli for suggestions, discussions, designs and help during the construction and the assembly of the FTU equilibrium magnetic measurements. Acknowledgements for suggestions, discussions and help during the debugging of these measurements and their interfacing with the data acquisition and archive systems are due to R. Bartiromo, G. Buceti, G. Bracco, M. Marinucci, G.B. Righetti, J. Snipes and M. Zoffoli. Also P. Buratti, O. Tudisco and M. Zerbini, for the ECE measurements, and M. Grolli, for the DCN interferometer measurements, have to be thanked for providing the data of their diagnostics with a reliability without which this work would not have been possible. F. Crisanti has to be thanked for the common work with one of the authors of this paper in the development of the first version of the Zernicke density inversion code, which was developed and applied to the JET experiment in 1987. Finally, a particular acknowledgement is due to the team that has operated the FTU tokamak and that has produced all the plasmas investigated in this paper, i.e. to G. Apruzzese, F. Crisanti, D. Frigione, H. Kroegler, L. Lovisetto, G. Mazzitelli and S. Podda.

REFERENCES

[1] ALLADIO, F., CRISANTI, F., Nucl. Fusion **26** (1986) 1143.
[2] CHRISTIANSEN, J.P., TAYLOR, J.B., Nucl. Fusion **22** (1982) 111.
[3] LUXON, J.L., BROWN, B.B., Nucl. Fusion **22** (1982) 813.
[4] LAO, L.L., et al., Nucl. Fusion **25** (1985) 1421.
[5] LAO, L.L., et al., Nucl. Fusion **25** (1985) 1611.
[6] LAO, L.L., et al., Nucl. Fusion **30** (1990) 1035.
[7] POWELL, E.T., et al., Nucl. Fusion **33** (1993) 1493.
[8] SEGRE, S.E., Plasma Phys. **20** (1978) 295.
[9] SOLTWISCH, H., Rev. Sci. Instrum. **57** (1986) 1939.
[10] HOFMANN, F., TONETTI, G., Nucl. Fusion **28** (1988) 1871.